Published in Contributions to Mineralogy and Petrology 155, issue 6, 703-717, 2008
which should be used for any reference to this work

Detrital, metamorphic and metasomatic tourmaline in high-pressure metasediments from Syros (Greece): intra-grain boron isotope patterns determined by secondary-ion mass spectrometry

Horst R. Marschall · Rainer Altherr · Angelika Kalt · Thomas Ludwig

Abstract The boron isotopic composition of zoned tourmaline in two metasediments from the island of Syros, determined by secondary-ion mass spectrometry (SIMS), reflects the sedimentary and metamorphic record of the rocks. Tourmaline from a silicate-bearing marble contains small ($\leq$20 μm) detrital cores with highly variable δ^{11}B values (-10.7 to $+3.6$‰), pointing to a heterogeneous protolith derived from multiple sources. The sedimentary B isotopic record survived the entire metamorphic cycle with peak temperatures of $\sim$500°C. Prograde to peak metamorphic rims are homogeneous and similar among all analysed grains (δ^{11}B $\approx$ +0.9‰). The varying δ^{11}B values of detrital cores in the siliceous marble demonstrate that in situ B isotope analysis of tourmaline by SIMS is a potentially powerful tool for provenance studies not only in sediments but also in metasediments. A meta-tuffitic blueschist bears abundant tourmaline with dravitic cores of detrital or authigenic origin (δ^{11}B ≈ -3.3‰), and prograde to peak metamorphic overgrowth zones (-1.6‰). Fe-rich rims, formed during influx of B-bearing fluids under retrograde conditions, show strongly increasing δ^{11}B values (up to +7.7‰) towards the margins of the grains. The δ^{11}B values of metamorphic tourmaline from Syros, formed in mixed terrigenous–marine sediments, reflect the B signal blended from these two different sources, and was probably not altered by dehydration during subduction.

Keywords Boron isotopes · Tourmaline · High-pressure · Metasediment · Subduction zone

H. R. Marschall (✉) · R. Altherr · T. Ludwig
Mineralogisches Institut, Universität Heidelberg,
Im Neuenheimer Feld 236, 69120 Heidelberg, Germany
e-mail: horst.marschall@bristol.ac.uk

H. R. Marschall
Department of Earth Sciences, University of Bristol,
Wills Memorial Building,
Queen's Road, Bristol BS8 1RJ, UK

A. Kalt
Institut de Géologie, Université de Neuchâtel,
Rue Emile Argand 11, 2007 Neuchâtel, Switzerland

Introduction

Tourmaline occurs in a variety of lithologies and is stable over an exceptionally large *P–T* range, including conditions in subducting slabs upto a depth of $\sim$250 km (Reinecke 1998; Werding and Schreyer 2002; Bebout and Nakamura 2003). Growth and stability of this widespread boro-silicate in subducting metasediments is thought to be responsible for recycling of B with an isotopic composition influenced by surface processes into the deep mantle. Previous B isotope studies on high-pressure metamorphic tourmaline have revealed important insights into B isotope fractionation within dehydrating subducting crust (Nakano and Nakamura 2001; Bebout and Nakamura 2003).

During sedimentary processes, tourmaline together with zircon and rutile is one of the most stable minerals (see Henry and Dutrow 2002, and references therein). It is enriched in highly mature sediments (Thiel 1941; Hubert 1962; Henry and Dutrow 2002), and is one of the most important minerals used in provenance studies (e.g. Lihou and Mange-Rajetzky 1996; Li et al. 2004; Mange and Otvos 2005; Morton et al. 2005). The chemical composition of detrital grains preserved in metasediments has commonly been used to investigate the provenance of the sedimentary protoliths (Henry and Guidotti 1985). The B

isotopic composition of tourmaline is a potentially powerful indicator in provenance studies of sediments and metasediments, given the extensive range of δ^{11}B values of tourmaline in natural rocks of $\sim$ 55‰ (Slack et al. 1993; Marschall et al. 2006).

Volume diffusion of major and trace elements and B isotopes in tourmaline is insignificant up to temperatures of 600°C (Henry and Dutrow 1994; Dutrow et al. 1999; Henry and Dutrow 2002; Bebout and Nakamura 2003). Therefore, chemical and isotopic heterogeneities of detrital grains, as well as metamorphic growth zones, are readily preserved even in rocks equilibrated in the amphibolite or low-*T* eclogite facies. In addition, tourmaline itself records the metamorphic evolution of the host rock by changing its major element composition, such as X_{Mg} and Ca/Na ratios. With future advancements in the investigation of the thermodynamic properties of tourmaline (e.g. van Hinsberg and Schumacher 2007), this has the potential for a quantification of the metamorphic *P–T* history of tourmaline in a specific sample, with a correlation to its B isotopic evolution.

Studies of various isotope systems in tourmaline have been successfully applied to decipher the fluid history of fluid-melt-rock systems (e.g. King and Kerrich 1989; Frei and Pettke 1996; Jiang 1998; Dyar et al. 1999; Slack 2002; Maloney 2007). The preservation of growth zones in hydrothermal and metamorphic tourmaline related to its slow intracrystalline diffusivity predestines tourmaline to be used as a key to the fluid–chemical history of metamorphic rocks. Thus, the internal B isotopic zonation of tourmaline grains can be employed as a reliable monitor for the B isotopic evolution of a rock throughout its pre-metamorphic and metamorphic history.

The development of the secondary-ion mass spectrometry (SIMS) technique for in situ analyses of B isotope ratios allows for detailed investigations of multiple zoned tourmaline (Smith and Yardley 1994; Chaussidon and Appel 1997; Nakano and Nakamura 2001; Bebout and Nakamura 2003; Altherr et al. 2004; Marschall et al. 2006; van Hinsberg and Marschall 2007). In this paper, we demonstrate that high-resolution B isotope analyses of high-pressure metasedimentary tourmaline from Syros (Greece) by SIMS enables us to discriminate detrital cores from prograde and retrograde growth zones.

Geology of Syros and occurrence of tourmaline

The major part of the island of Syros (Cyclades, Greece; Fig. 1) is composed of interlayered pelitic to psammitic schists and marbles with minor intercalations of quarzites, calc-schists and metaconglomerates (Hecht 1984; Dixon and Ridley 1987; Seck et al. 1996). They are interpreted as metamorphosed flysch sediments (Dixon and Ridley 1987) deposited during the Triassic and Jurassic (up to Cretaceous?) (Keay 1998; Bröcker and Pidgeon 2007).

The petrological, geochronological, structural and tectono-metamorphic evolution of the island of Syros has been investigated in a large number of studies (e.g. Dixon 1968; Ridley 1984; Rosenbaum et al. 2002; Brady et al. 2004; Keiter et al. 2004; Forster and Lister 2005; Bröcker and Keasling 2006). For different rock types, a prograde

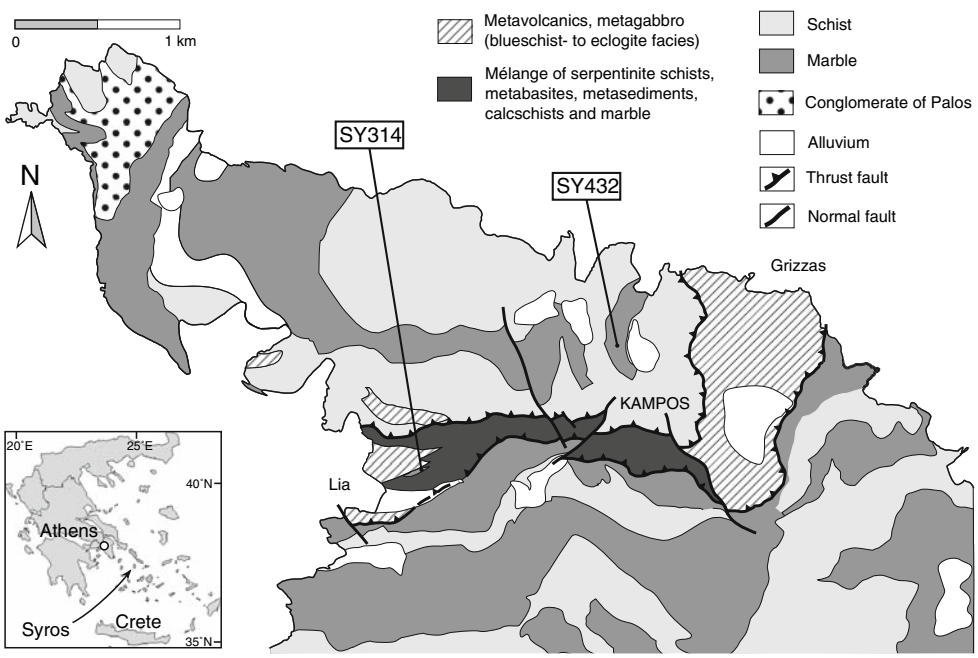

Fig. 1 Simplified geological map of the northern part of Syros (after Keiter et al. 2004). SY314 was sampled from a lens of meta-sedimentary schist within the Kampos mélange, while SY432 was sampled from an outcrop of layered marbles north of the mélange. The *inset* shows a map of Greece with the location of the island of Syros

P–T path was derived, characterised by a high *P*/*T* ratio, typical for subduction zone metamorphism. Metamorphic peak conditions were estimated to be ~470–520°C and 1.3–2.0 GPa (Dixon 1968; Ridley 1984; Okrusch and Bröcker 1990; Trotet et al. 2001; Rosenbaum et al. 2002; Keiter et al. 2004). A number of U–Pb TIMS and SHRIMP data from zircon, Lu–Hf data from garnet and $^{40}Ar/^{39}Ar$ data from white mica and glaucophane are now available and have been used to date the evolution of Syros H*P* rocks. Subduction and high-pressure metamorphism most probably occurred in the Eocene (~54–50 Ma) (Maluski et al. 1987; Tomaschek et al. 2003; Lagos et al. 2003; Forster and Lister 2005), although an additional pre-Eocene high-pressure event at ~80 Ma was suggested by Bröcker and co-workers (Bröcker and Enders 2001; Bröcker and Keasling 2006). In some parts of Syros, formations are composed of blocks of meta-igneous and metasedimentary rocks embedded in a matrix of chlorite schist and serpentinite, referred to as "mélanges" (Dixon 1968; Hecht 1984; Dixon and Ridley 1987; Okrusch and Bröcker 1990; Seck et al. 1996; Bröcker and Enders 2001; Marschall et al. 2006). The exhumation path of the Syros high-pressure rocks is characterised by near-isothermal decompression at ~400°C, with a preservation of the H*P* assemblages and minerals in many parts of the island, but variable rehydration during exhumation (Trotet et al. 2001; Marschall et al. 2006).

Tourmaline in Syros H*P* metamorphic rocks is related to two different occurrences, which can be distinguished petrographically. Type-I is found dominantly within metasedimentary rocks as small (≤100 μm in cross-section) complexly zoned crystals, typically occurring as inclusions in garnet, glaucophane or phengite. Type-II appears as aggregates of large (0.1–15 mm in cross-section), relatively homogeneous grains and is clearly related to metasomatism during exhumation of the rocks (Marschall et al. 2006). It is restricted to hydrous reaction zones formed at the contact between blocks and the ultramafic matrix of the mélange. Type-II tourmaline grew at the expense of retrograde glaucophane and chlorite during rehydration and exhumation. It shows exceptionally high $\delta^{11}B$ values exceeding +18‰ in all samples (Marschall et al. 2006). The formation process, chemistry and B isotopic composition of Type-II tourmaline are discussed in detail in Marschall et al. (2006). This paper deals with the genesis, chemistry and B isotopic composition of Type-I tourmaline in rock samples that show only limited influence of metasomatism and reaction with the ultramafic portion of the mélange. Two metasedimentary samples (SY314 and SY432) have been recognised to contain abundant Type-I tourmaline, which was analysed in detail for major element composition by EPMA and for B isotopic composition by SIMS.

Investigated samples

Phengite–glaucophane schist SY314

Sample SY314 is a meta-sedimentary glaucophane schist from the northern mélange, approximately 250 m W of Kámpos (37°29′28″N; 24°54′17″E; Fig. 1), close to *Monolith I* of Dixon and Ridley (1987). The sample was taken from a glaucophane-schist lens with a foliation concordant to the dominant foliation of the mélange. The contact of the schist with the ultramafic matrix is characterised by metasomatic reaction zones. Sample SY314, which was taken from the centre of the schist lens, consists of (ferro-)glaucophane, phengite, garnet and accessory apatite, titanite, epidote, quartz, tourmaline and Fe-oxide. Tourmaline occurs as small euhedral grains, 50–100 μm in cross-section as inclusions in glaucophane porphyroblasts and in the phengite-rich matrix (Fig. 2a–d). Many tourmaline grains have anhedral poikiloblastic cores, overgrown by three zones (Figs. 2, 3) that differ by colour intensity in optical images from light green near the core to dark green at the edges. Inclusions of Fe-oxide (?) in poikiloblastic cores are typically ≤1 μm.

SY314 displays prograde zonation of minerals, such as garnet and Na-amphibole, a H*P* metamorphic assemblage of glaucophane + garnet (~15% Prp) + phengite, and clear evidence for retrograde reactions, such as the formation of albite, stilpnomelane and Ca-amphibole from glaucophane (Fig. 2a), Fe-rich rims on tourmaline, garnet and glaucophane, and biotite after phengite (Fig. 2d). However, most parts of the minerals are unaltered and still display their prograde and peak-metamorphic compositions. These observations suggest a restricted influx of hydrous fluid into the rock during retrograde metamorphic conditions.

On the basis of mineral and whole-rock major- and trace-element analyses, the rock has been interpreted as the metamorphic equivalent of a tuffitic marine sediment mixed with continental detritus (Marschall 2005). Elevated contents of MnO (1.0wt%), K_2O (2.3wt%), SiO_2 (54wt%) and B (94 μg/g) with respect to MORB are explained by exposure of the former tuffite to seafloor alteration, which typically leads to the formation of Fe–Mn hydroxides, clay minerals and opal or chalcedony (e.g. Alt et al. 1986).

Siliceous marble SY432

Sample SY432 is a fine-grained, well-foliated siliceous marble from the schist-and-marble sequence north of the Kambos mélange. The sample locality is an outcrop of several tens of metres of a layered marble sequence, which is located on the north-eastern slope of the island, ~250 m N of Kambos (37°29′53″N; 24°55′03″E; Fig. 1). The rock

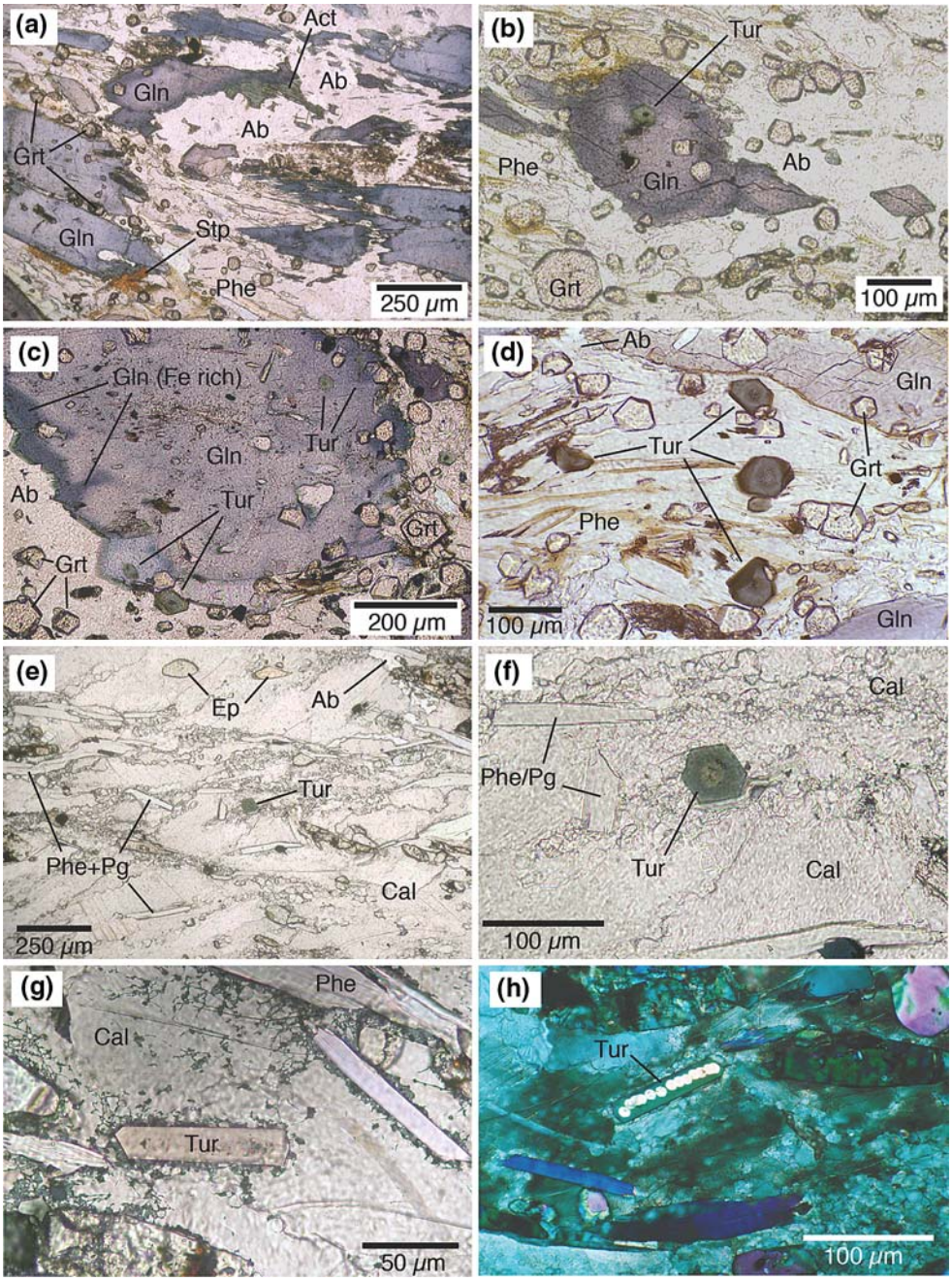

Fig. 2 Photomicrographs of Phe-Gln schist SY314 (**a**–**d**) and siliceous marble SY432 (**e**–**h**). All images were taken in plane-polarised light, except for **h** (crossed polarisers). **a** Replacement of Gln by Ca-rich amphibole (Act), Ab and Stp. **b** Tur and Grt inclusions in Gln. **c** Several Tur grains included in and surrounding Gln displaying a *dark* (Fe-rich) rim. **d** Several zoned Tur grains with poikiloblastic cores and *dark* (Fe-rich) rims. Phe display (*dark*) *brown* rims (transformation to Bt). **e** Microstructure of siliceous marble SY432 with Ep, white mica, Tur and some secondary Ab in a Cal matrix. **f** Tur grain with *bright*, *rounded* core and *dark*, euhedral, homogeneous rim. **g** Euhedral Tur grain "C" cut parallel to the crystallographic c-axis (polariser E-W). **h** Grain C after being analysed with SIMS. The section is still covered by the gold layer with the analysis sites visible as *bright* spots. Mineral abbreviations after Kretz (1983): *Ab* albite, *Act* actinolite, *Cal* calcite, *Ep* epidote, *Gln* glaucophane, *Grt* garnet, *Pg* paragonite, *Phe* phengite, *Stp* stilpnomelane, *Tur* tourmaline

consists of calcite, epidote, quartz, phengite, paragonite, apatite, zircon and small euhedral tourmaline grains of 50–100 μm in cross section (Fig. 2). Secondary albite, hematite and chlorite are rare. Tourmaline grains show anhedral poikiloblastic cores overgrown by euhedral, homogeneous rims (Figs. 2f, 4). The rock is interpreted as a former carbonate-rich sediment diluted by silicate detritus (probably clay minerals, feldspar and quartz).

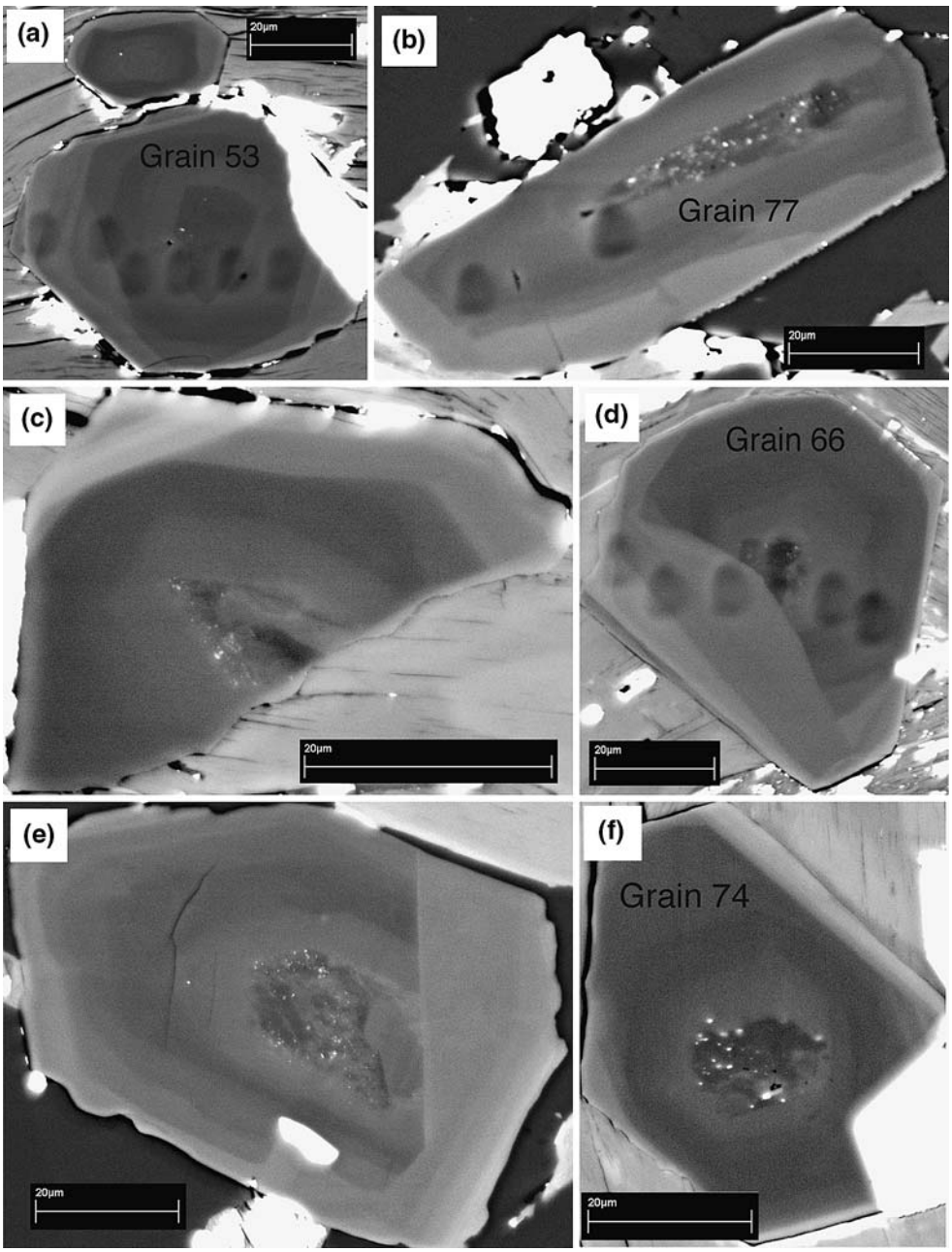

Fig. 3 Back scattered electron (BSE) images of individual tourmaline grains in sample SY314 displaying poikiloblastic cores and different growth zones. Fe-rich rims (*bright zones*) are visible on most grains. *Dark spots* in **a**, **b** and **d** are spots from SIMS analysis. *Scale bar* in all pictures is 20 µm

Analytical methods

Compositions of mineral phases were determined using a Cameca SX 51 electron microprobe equipped with five wavelength-dispersive spectrometers (Mineralogisches Institut, Heidelberg). Operating conditions were 20 nA beam current and 15 kV acceleration voltage. For analyses of micas, the electron beam was defocused to 10 µm in order to avoid loss of alkalis. For analyses of tourmaline it was defocused to 5 µm. For tourmaline, a modified matrix correction was applied assuming stoichiometric oxygen and all non-measured components to be B_2O_3. The accuracy of the electron microprobe analyses of tourmaline and the correction procedure was checked by measuring three samples of reference tourmalines (98144: elbaite, 108796: dravite, 112566: schorl; Dyar et al. 1998, 2001). Analytical errors on all analyses are $\pm 1\%$ relative for major elements and $\pm 5\%$ for minor elements. A detailed description of the applied electron microprobe techniques for tourmaline analysis is given elsewhere (Kalt et al. 2001).

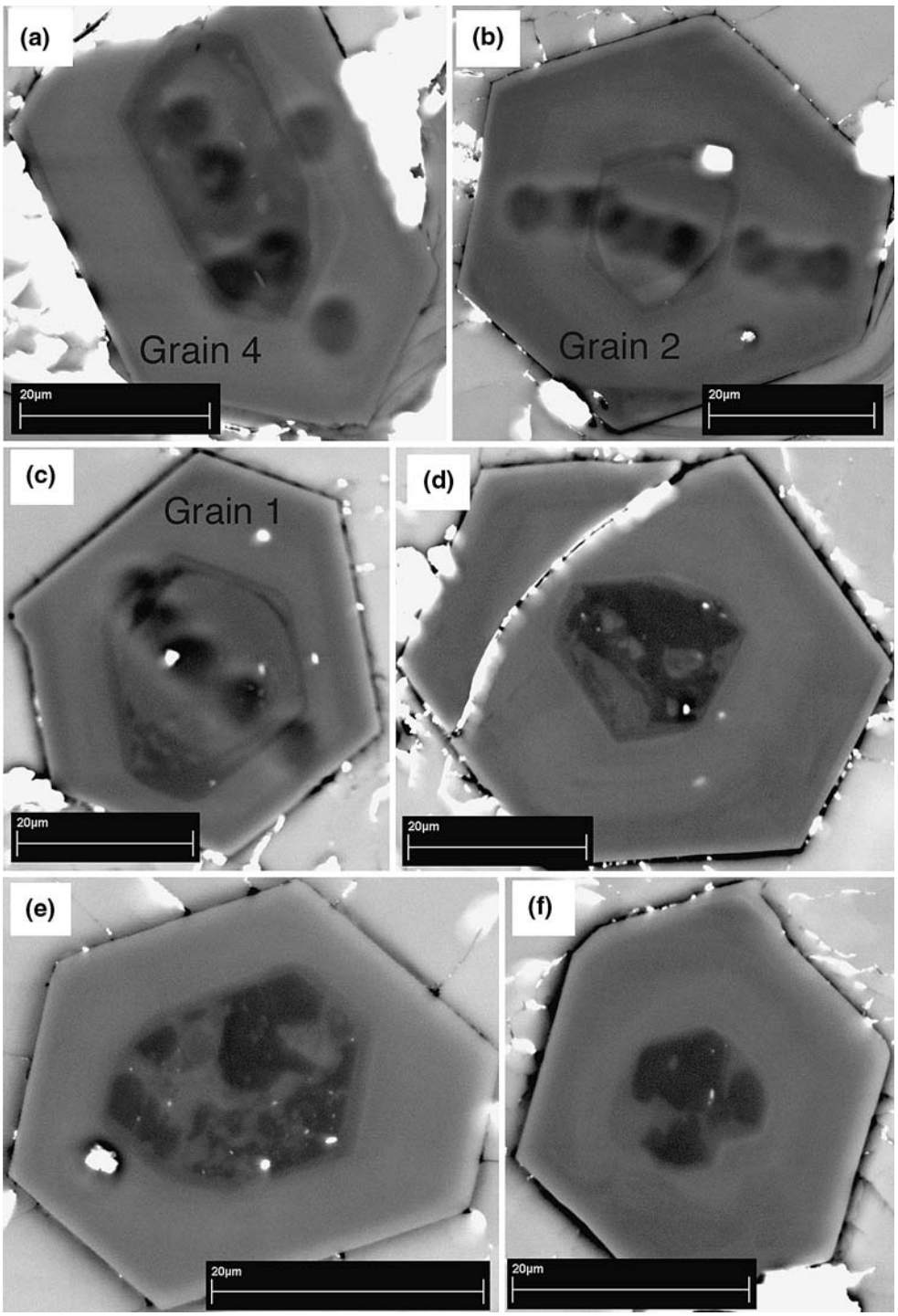

Fig. 4 BSE images of individual tourmaline grains in sample SY432 displaying *rounded* and *patchy* cores and homogeneous rims. *Dark spots* in **a**, **b** and **c** are spots from SIMS analysis. *Scale bar* in all pictures is 20 µm

Boron isotope ratios of tourmaline and phengite were measured by secondary ion mass spectrometry (SIMS) with a modified Cameca IMS 3f ion microprobe at the Mineralogisches Institut, Heidelberg. Primary ion beam was $^{16}O^{-}$ accelerated to 10 keV with a beam current of 1 nA, resulting in count rates for ^{11}B of $\sim 2 \times 10^5$ s^{-1} and $\sim 5 \times 10^4$ s^{-1} for ^{10}B on tourmaline, collected by a single electron multiplier. Diameter of the 1 nA spot ranged from 5 to 10 µm mainly depending on the operating duration of the ion source. The energy window was set to 50 eV and no offset was applied. Each analysis consisted of 50 cycles with counting times of 3.307 and 1.660 s on ^{10}B and ^{11}B,

respectively. Presputtering lasted for 5 min and settling time between two different masses was 200 ms, resulting in total analysis time for one spot of approximately 10 min. Internal precision of a single analysis was $\leq$1‰ (2σ). Boron isotopic compositions of samples are reported in delta notation (δ^{11}B in ‰) relative to the SRM 951 certified value (Catanzaro et al. 1970). Instrumental mass fractionation was corrected by using three samples of proposed reference tourmaline (98114: elbaite, 108796: dravite, 112566: schorl; Leeman and Tonarini 2001). Long-term reproducibility of measured isotope ratios on these standard tourmalines was $\pm$1.0‰ (2σ). A total of 56 B isotope analyses on tourmaline were completed (Table 1). Further details on boron isotope analysis at the SIMS facility in Heidelberg are given elsewhere (Marschall 2005; Marschall and Ludwig 2006; Marschall et al. 2006).

Contents of H_2O and B_2O_3 were calculated stoichiometrically (OH + F + Cl = 4 pfu, B = 3 pfu). Li and Be were assumed to be negligible. These assumptions are justified by SIMS analyses on sample SY314 using $\sim$30 μm spots (averaging large parts of tourmaline grains). They revealed B_2O_3 concentrations of 10.14wt%, and Li and Be concentrations of 8.6 and 0.37 μg/g, respectively (Marschall 2005).

Results

All investigated tourmalines belong to the schorl–dravite solid solution series with some Ca-rich domains, representing an uvite component of up to 25 mole%. Most of the tourmaline is Mg-rich (dravitic; $X_{Mg} \approx$ 0.6–0.8). In detail, tourmaline grains of the two samples display chemical (Mg-Fe-Ca-Ti-F) and B isotopic zonations, which are crucial for the interpretation of the B isotopic history of the rocks.

Tourmaline in sample SY314 displays significant chemical differences between the zones that are visible under the optical microscope. Anhedral poikiloblastic cores have very low Ca ($\sim$0.01 pfu), F (<0.1 pfu) and TiO_2 (<0.1wt%) concentrations and relatively high X_{Mg} (0.68; Fig. 5 and Table 1). No differences in chemical composition were observed between poikiloblastic cores of different grains. Euhedral homogeneous cores, some of which overgrew poikiloblastic cores show relatively high Ca ($\sim$0.05 pfu) and F ($\sim$0.2 pfu) contents but are still low in TiO_2 ($\leq$0.25wt%; Fig. 5 and Table 1). All analysed grains are characterised by strongly decreasing X_{Mg} and Ca contents from homogeneous cores to mantle to rim at the edge of the crystals, while F contents are more or less constant (Fig. 5 and Table 1). Most analyses of rims reveal schorl rather than dravite with X_{Mg} as low as $\sim$0.35.

Boron isotope analyses also revealed systematic differences among the different zones. Poikiloblastic cores of the three analysed grains are indistinguishable within error with δ^{11}B values of -3.3 ± 1.8‰ (Fig. 5 and Table 1). Euhedral homogeneous cores show δ^{11}B values of -1.6 ± 1.1‰ (six grains) and mantles show values of $+0.7 \pm 1.7$‰ (three grains). Within Fe-rich rims, the δ^{11}B values of all analysed grains strongly increase outwards, and reach values as high as +7.7‰ (Fig. 5 and Table 1).

In sample SY432, poikiloblastic cores of tourmaline grains display strong chemical differences from one grain to another. Ca, Ti and F contents as well as X_{Mg} are very different among different cores (Fig. 6 and Table 1). The rims on the other hand, are homogeneous and all chemically similar, with dravitic composition. They contain $\sim$0.25–0.45 apfu F, display Ca/(Ca + Na) ratios of $\sim$0.09 and X_{Mg} of $\sim$0.64 (Fig. 6). Cr and Zn contents of most cores are below the detection limits of EPMA, while rims show elevated concentrations of both elements (Table 1). Fe-rich rims were not observed in tourmaline from sample SY432.

Boron isotope analyses of cores from different tourmaline revealed strongly contrasting δ^{11}B values, ranging from -10.7 ± 1.1 to -2.8 ± 1.6 to $+3.6 \pm 1.5$‰ (Fig. 6 and Table 1). The chemically homogeneous and similar rims of all analysed grains display nearly constant δ^{11}B of $+0.9 \pm 1.8$‰ (Fig. 6 and Table 1). At the boundaries between cores and rims, SIMS analyses revealed δ^{11}B values intermediate between core and rim. In principle, these could be artefacts of the SIMS spot overlapping the two contrasting zones, or true values resulting from diffusional re-equilibration between the two zones during metamorphism. The major element profiles determined by EPMA and the sharp boundaries in the BSE images (Fig. 4), which both provide a higher lateral resolution than SIMS, do not show evidence for diffusional equilibration between cores and rims. Therefore, intermediate δ^{11}B values should be interpreted as analytical artefacts. Increasing δ^{11}B values at the rims of tourmaline (as in sample SY314) were not observed in sample SY432.

Discussion

Previous studies on δ^{11}B variations in high-pressure metasedimentary tourmaline

Nakano and Nakamura (2001) investigated tourmaline from a series of metasediments (metapelites and metapsammites) from the Sambagawa belt. They observed strongly zoned tourmaline with δ^{11}B values decreasing from -3‰ in the core to -10‰ at the rim within single grains. Mg contents steadily increase from core to rim, due

Table 1 Representative chemical analyses and average of B isotopic analyses of tourmaline from Syros metasediments

Sample	SY314												SY432							
Type	Poikiloblastic core			Core			Mantle			Rim			Core				Rim			
Grain no.	95	66	70	85	85	70	66	53	66	74	12	70	1	2	4	6	1	2	4	6
SiO_2	35.90	35.79	35.66	35.85	35.68	35.57	35.19	35.28	35.69	35.09	34.47	34.53	34.81	35.10	36.28	35.94	35.57	35.74	35.57	35.45
TiO_2	0.08	0.12	0.07	0.19	0.25	0.19	0.49	0.17	0.20	0.55	1.00	0.93	0.28	1.00	0.05	0.06	0.22	0.23	0.24	0.27
$B_2O_3^a$	10.41	10.38	10.38	10.39	10.32	10.30	10.22	10.31	10.30	10.17	9.98	10.01	10.22	10.47	10.58	10.41	10.31	10.34	10.34	10.38
Al_2O_3	30.55	30.45	31.08	29.31	29.50	29.10	29.03	29.38	28.95	28.44	27.64	28.14	29.14	31.35	31.72	30.04	29.60	29.51	29.42	29.83
Cr_2O_3	0.04	0.01	0.02	0.07	0.01	0.05	0.03	0.04	0.04	0.10	0.07	0.09	0.09	0.04	0.02	0.05	0.11	0.11	0.09	0.06
FeO^t	6.98	6.99	6.40	7.86	7.89	7.88	10.15	7.09	7.52	11.53	14.37	13.77	7.90	6.99	4.82	6.29	7.75	7.78	8.07	7.92
MnO	0.20	0.18	0.19	0.00	0.10	0.02	0.05	0.06	0.02	0.00	0.09	0.08	0.02	0.03	0.04	0.02	0.07	0.00	0.02	0.05
MgO	8.12	7.98	7.91	8.58	7.92	8.51	6.72	8.95	8.60	6.26	4.23	4.23	7.96	7.43	9.11	9.00	7.67	7.86	8.00	7.90
CaO	0.08	0.12	0.04	0.40	0.23	0.36	0.15	0.44	0.38	0.25	0.14	0.10	1.00	1.33	0.13	0.22	0.53	0.53	0.52	0.69
ZnO	0.00	0.06	0.03	0.07	0.05	0.08	0.09	0.03	0.06	0.07	0.01	0.00	0.16	0.05	0.05	0.02	0.09	0.14	0.15	0.15
Na_2O	2.80	2.74	2.66	2.87	2.83	2.65	2.87	2.80	2.80	2.76	2.82	2.87	2.74	1.98	2.69	2.80	2.84	2.84	2.82	2.94
K_2O	0.00	0.01	0.02	0.01	0.01	0.02	0.01	0.04	0.03	0.02	0.03	0.07	0.01	0.04	0.02	0.02	0.03	0.02	0.03	0.01
H_2O^a	3.52	3.49	3.52	3.46	3.44	3.43	3.37	3.39	3.42	3.39	3.34	3.36	3.16	3.46	3.53	3.21	3.19	3.23	3.18	3.23
F	0.16	0.18	0.13	0.27	0.25	0.26	0.33	0.36	0.28	0.26	0.21	0.20	0.76	0.32	0.26	0.79	0.77	0.71	0.81	0.73
Cl	0.00	0.00	0.01	0.00	0.00	0.01	0.00	0.00	0.01	0.00	0.00	0.00	0.00	0.00	0.00	0.01	0.01	0.00	0.00	0.00
$-(F + Cl) = O$	0.07	0.08	0.06	0.11	0.10	0.11	0.14	0.15	0.12	0.11	0.09	0.09	0.32	0.13	0.11	0.34	0.33	0.30	0.34	0.31
Total	98.76	98.43	98.05	99.22	98.36	98.30	98.56	98.18	98.18	98.78	98.31	98.30	97.93	99.46	99.20	98.56	98.42	98.74	98.91	99.29
Formulas calculated to 31 oxygens, $Fe^{2+} = Fe^t$																				
Si	5.99	5.99	5.97	5.99	6.01	6.00	5.99	5.95	6.02	6.00	6.00	5.99	5.92	5.83	5.96	6.00	6.00	6.01	5.98	5.94
Ti	0.01	0.02	0.01	0.02	0.03	0.02	0.06	0.02	0.03	0.07	0.13	0.12	0.04	0.13	0.01	0.01	0.03	0.03	0.03	0.03
B	3.00	3.00	3.00	3.00	3.00	3.00	3.00	3.00	3.00	3.00	3.00	3.00	3.00	3.00	3.00	3.00	3.00	3.00	3.00	3.00
Al	6.01	6.01	6.13	5.78	5.86	5.79	5.82	5.84	5.76	5.73	5.67	5.76	5.84	6.14	6.14	5.91	5.88	5.85	5.83	5.89
Cr	0.01	0.00	0.00	0.01	0.00	0.01	0.00	0.01	0.01	0.01	0.01	0.01	0.01	0.01	0.00	0.01	0.01	0.01	0.01	0.01
Fe^{2+}	0.97	0.98	0.90	1.10	1.11	1.11	1.44	1.00	1.06	1.65	2.09	2.00	1.12	0.97	0.66	0.88	1.09	1.09	1.14	1.11
Mn	0.03	0.03	0.03	0.00	0.01	0.00	0.01	0.01	0.00	0.00	0.01	0.01	0.00	0.01	0.01	0.00	0.01	0.00	0.00	0.01
Mg	2.02	1.99	1.98	2.14	1.99	2.14	1.70	2.25	2.16	1.59	1.10	1.10	2.02	1.84	2.23	2.24	1.93	1.97	2.01	1.97
Ca	0.01	0.02	0.01	0.07	0.04	0.07	0.03	0.08	0.07	0.05	0.03	0.02	0.18	0.24	0.02	0.04	0.10	0.10	0.09	0.12
Zn	0.00	0.01	0.00	0.01	0.01	0.01	0.01	0.00	0.01	0.01	0.00	0.00	0.02	0.01	0.01	0.00	0.01	0.02	0.02	0.02
Na	0.90	0.89	0.86	0.93	0.93	0.87	0.95	0.91	0.92	0.92	0.95	0.97	0.90	0.64	0.86	0.91	0.93	0.93	0.92	0.96
K	0.00	0.00	0.00	0.00	0.00	0.01	0.00	0.01	0.01	0.00	0.01	0.02	0.00	0.01	0.00	0.00	0.01	0.00	0.01	0.00
Total	18.95	18.93	18.89	19.05	18.99	19.02	19.02	19.07	19.03	19.02	19.00	18.99	19.07	18.80	18.89	18.99	18.99	19.00	19.03	19.06
X_{Mg}	0.675	0.670	0.688	0.661	0.641	0.658	0.541	0.692	0.671	0.492	0.344	0.354	0.643	0.655	0.771	0.718	0.638	0.643	0.639	0.640
OH	3.91	3.90	3.93	3.86	3.87	3.86	3.82	3.81	3.85	3.86	3.89	3.89	3.59	3.83	3.87	3.58	3.59	3.62	3.57	3.61

Table 1 continued

Sample	SY314										SY432									
Type	Poikiloblastic core			Core		Mantle		Rim			Core				Rim					
Grain no.	95	66	70	85	85	70	66	53	66	74	12	70	1	2	4	6	1	2	4	6
F	0.09	0.10	0.07	0.14	0.13	0.14	0.18	0.19	0.15	0.14	0.12	0.11	0.41	0.17	0.13	0.42	0.41	0.38	0.43	0.39
Cl	0.00	0.00	0.00	0.00	0.00	0.00	0.00	0.00	0.00	0.00	0.00	0.00	0.00	0.00	0.00	0.00	0.00	0.00	0.00	0.00

Boron isotope values (averages of SIMS analyses)

	SY314					SY432 core				SY432 rim			
	Poikiloblastic core	Core	Mantle	Rim		Grain 1	Grain 2	Grain 4	Grain 6	Grain 1	Grain 2	Grain 4	Grain C
δ^{11}B	−3.3	−1.6	+0.7	+5.4[b]		−2.8	−10.7[c]	+3.6	n.a.	+1.8	+0.7	+0.7	+0.8
$2RSD_{mean}$	1.8	1.1	1.7	3.9[b]		1.6	1.1[c]	1.5		2.2	0.9	1.8	2.0
n	6	8	4	4		3	2[c]	4		2	5	2	13

n number of isotope analyses

[a] H_2O and B_2O_3 calculated stoichiometrically. All other elements analysed by EPMA. Analyses sums short of 100% may point to certain amounts of trivalent Fe and/or tetrahedral B

[b] Rim zone of sample SY314 shows B isotopic zonation (see Fig. 5) with δ^{11}B increasing from +3.3 to +7.7‰

[c] Only analyses of centre of core of grain number 4 are listed

to tourmaline growth during increasing temperatures. The authors explain the B isotope zonation patterns by B isotopic fractionation between mica, fluid and tourmaline in the following way: δ^{11}B values of tourmaline cores are higher than δ^{11}B values of the surrounding mica. At the beginning of metamorphic tourmaline growth, ^{11}B is preferentially released from mica and transported via fluids along grain boundaries and concentrated in tourmaline cores. The remaining mica is isotopically lighter and releases B with progressively lower δ^{11}B value into the fluid during further heating. Consequently, the growing tourmaline incorporates the lower ^{11}B/^{10}B ratio of the surrounding fluid, without re-equilibrating earlier growth zones. Thus, the B isotopic composition of a fluid phase within the metasediments during any one stage of metamorphism is recorded in the respective growth zone of tourmaline.

In a second study, Bebout and Nakamura (2003) investigated (U)H*P* metamorphic rocks from the Catalina Schist, California (USA) and from Lago di Cignana, Western Alps (Italy). Tourmaline grains from Catalina display decreasing δ^{11}B values (from −7 to −15‰) and increasing X_{Mg} from cores to rims, similar to the Sambagawa samples. At the outermost rims (∼30 μm), δ^{11}B values increase again to −7‰ concomitant with a decrease in X_{Mg}. Following Nakano and Nakamura (2001), Bebout and Nakamura (2003) attribute the core-to-rim decrease in δ^{11}B values to prograde redistribution of B from mica into growing tourmaline, and the increase of δ^{11}B at the outer rims to growth of tourmaline during influx of B-rich fluids at retrograde metamorphic conditions. Tourmaline grains from Lago di Cignana display homogeneous X_{Mg} and B isotopic compositions of −10‰ in cores and again a strong increase of δ^{11}B values within the outermost 100 μm accompanied by a decrease in X_{Mg}. According to the authors, the homogeneous core resulted from intra-grain diffusive re-equilibration of B isotopes at peak-metamorphic temperatures, which were higher for these samples (∼620°C) than in the other localities. Decrease of X_{Mg} and increase of δ^{11}B values to +4‰ again resulted from retrograde influx of B by fluids. In the case of Lago di Cignana, this interpretation is strongly supported by inclusions of coesite, garnet and rutile in the low δ^{11}B cores and of quartz and epidote in the high δ^{11}B rims.

Tourmaline in phengite–glaucophane schist SY314

Tourmaline in phengite–glaucophane schist SY314 shows poikiloblastic, rounded cores, which are different in chemical and B isotopic composition from all other zones. Stemming from the early or pre-metamorphic history of the rock, the poikiloblastic core tourmaline could be of two

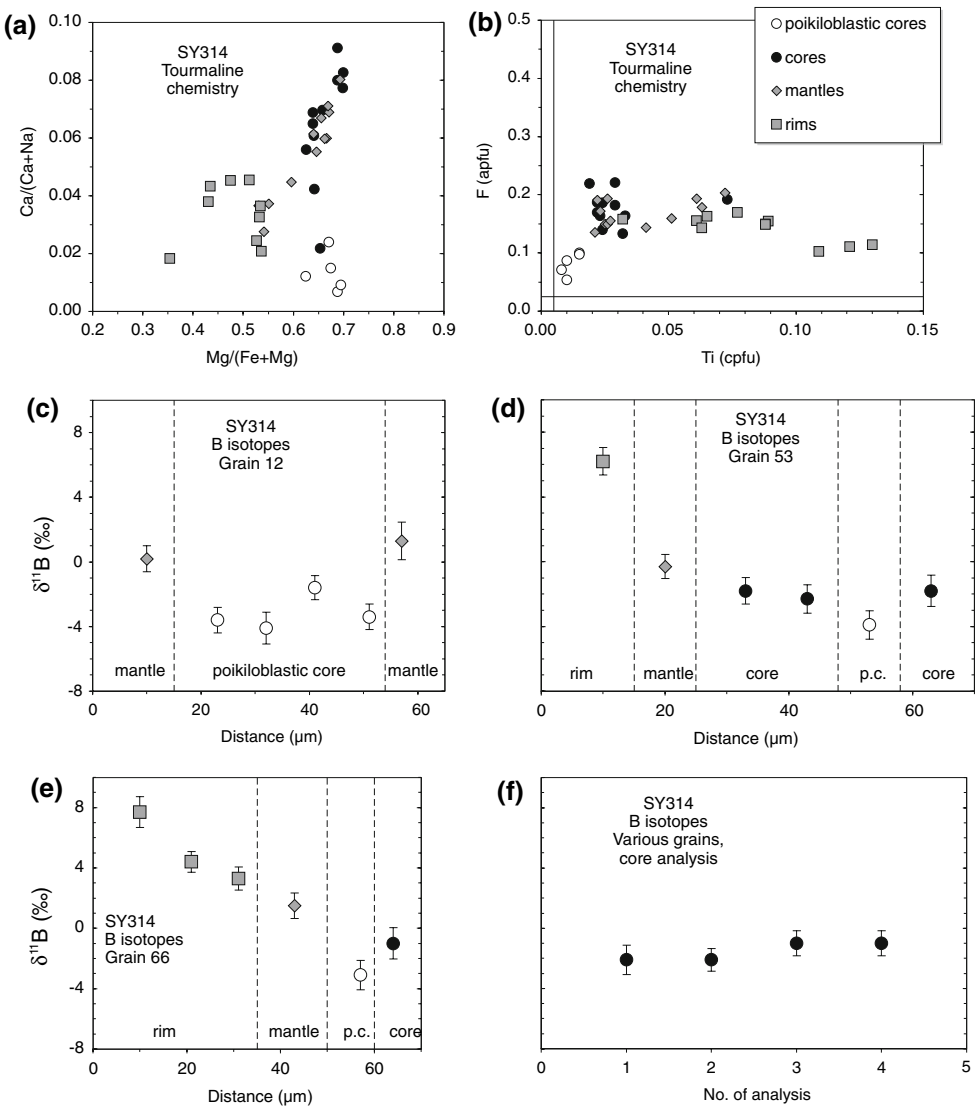

Fig. 5 **a–b** Chemical composition of tourmaline in sample SY314 showing four different zones of several grains. **a** Ca/(Ca + Na) versus Mg/(Mg + Fe). **b** F versus Ti (*solid lines* detection limits of EPMA). **c–e** B isotope traverses over different grains showing four different zones: *p.c.* poikiloblastic cores, cores, mantles and rims, as distinguished by optical and chemical differences. **f** B isotope values of core analyses of different tourmaline grains of sample SY314

possible origins. They could represent detritus from a source supplying tourmaline with relatively homogeneous isotopic composition ($\delta^{11}B = -3.3‰$) and major element chemistry (low-Ca–Ti–F dravite). This hypothesis would explain the rounded shape and the slightly exotic chemical and isotopic composition compared to the other tourmaline growth zones. On the other hand, poikiloblastic grains are mechanically weaker and are, therefore, less likely to survive transport over large distances. Alternatively, the poikiloblastic cores could have formed by authigenic or epigenetic processes, i.e. within the un-solidified sediment during its exposure to B-bearing solutions at the seafloor. Previously reported $\delta^{11}B$ values of tourmaline formed during marine hydrothermal activity range from approximately −15 to 0‰ (Palmer 1991). This type of tourmaline is reported to display dravitic compositions (Slack 2002). The rounded shape of the poikiloblastic cores could, in that case, be explained by a stage of tourmaline dissolution in the history of the metamorphic rock.

The highest X_{Mg} and Ca contents of tourmaline in this sample are displayed by the euhedral Mg-rich cores and euhedral Mg-rich overgrowths on the anhedral poikiloblastic cores. These Mg-rich core zones are interpreted to have grown from mica-derived B during prograde and/or peak metamorphism, similar to the cases described by Nakano and Nakamura (2001) and Bebout and Nakamura (2003). A prograde zonation with a core-to-rim decrease in $\delta^{11}B$ was not observed in SY314, probably due to analytical limitations through small grain size and zoning. However, the $\delta^{11}B$ value of −1.6‰ in these core zones is interpreted to represent the last prograde growth zone of tourmaline in sample SY314 (Fig. 7). They show the highest Ca and Mg contents and are included in glaucophane blasts, as well as in phengite. The actual chemistry

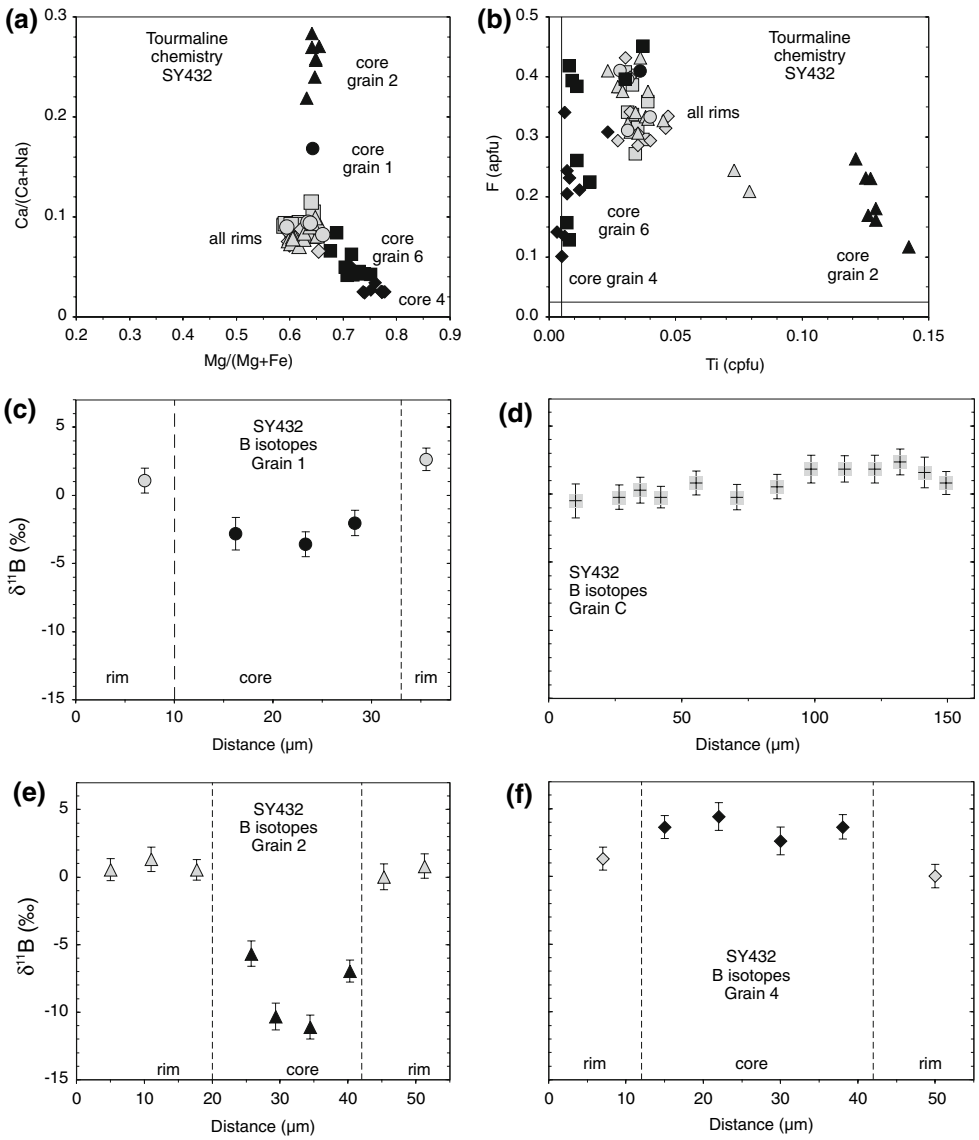

Fig. 6 **a–b** Chemical composition of tourmaline in sample SY432 showing cores (*black*) and rims (*grey*) of four individual grains (see also Fig. 4 and Table 1): grain 1 (*circles*), grain 2 (*triangles*), grain 4 (*diamonds*) and grain 6 (*squares*). Note that rim compositions of all grains are similar, while core compositions differ significantly. **a** Ca/(Ca + Na) versus Mg/(Mg + Fe). **b** F versus Ti (*solid lines* detection limits of EPMA). **c–f** B isotope traverses over different grains in sample SY432 showing cores (*black*) and rims (*grey*) of grains 1, C, 2 and 4. Grain C is a grain cut parallel to its crystallographic c-axis (see Fig. 2g)

of tourmaline is of course dependent on the chemical composition of the rock in which it formed, and may, for example, be more Ca-rich in marbles than in metapelites (Henry and Dutrow 2002), but it also varies with the *P–T* conditions of formation. In general, Ca and Mg contents of tourmaline increase with metamorphic grade in all kinds of lithologies (Henry and Dutrow 2002).

Towards the rims, Ca and Mg contents of tourmaline in the phengite-rich matrix decrease, while Ti and Fe contents increase significantly, which is interpreted as a result of tourmaline growth during decreasing temperatures. Retrograde growth of tourmaline requires influx of external B, which must have had a very high δ^{11}B value of at least +7.7‰ in the case of sample SY314, as recorded by the Fe-rich rims of tourmaline. Retrograde influx of hydrous fluid is also documented by other petrographic evidence, such as Fe-rich rims and streaks in garnet and glaucophane and the formation of stilpnomelane and biotite/chlorite at the expense of phengite. Tourmaline, in contact with hydrous fluids at high pressures probably shows no or very little B-isotope fractionation (Palmer and Swihart 2002; Marschall et al. 2006; Meyer et al. 2007). The retrograde influx of fluids carrying isotopically heavy B has been demonstrated earlier for rocks of the Syros mélange (Marschall et al. 2006). This process of rehydration during exhumation led to the precipitation of Type-II high-δ^{11}B tourmaline in the strongly metasomatised zones of the mélange (Marschall et al. 2006) and may also have formed the rims of Type-I tourmaline in sample SY314. Influx of high-δ^{11}B fluids, which led to retrograde tourmaline formation occurred during and after the formation of chlorite and albite (Marschall et al. 2006, Fig. 7).

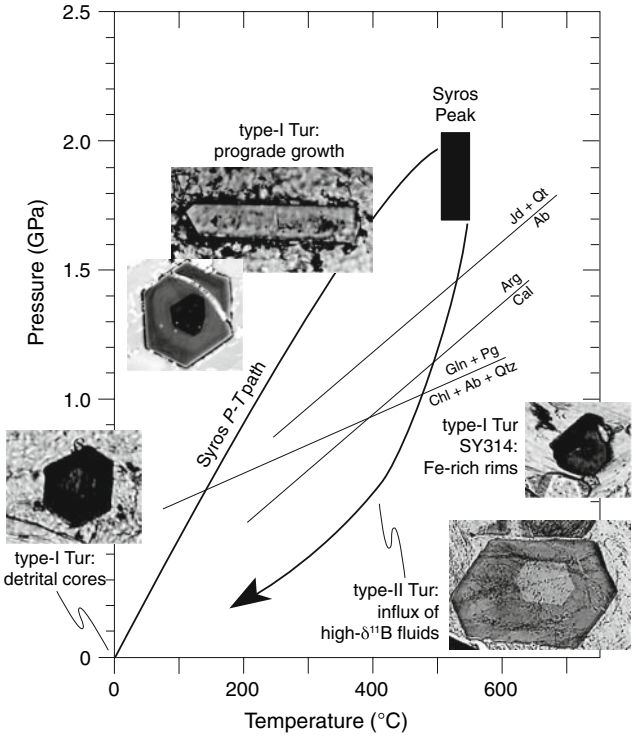

Fig. 7 Prograde and retrograde *P–T* path of Syros HPM rocks (after Marschall et al. 2006, and references therein). Ca–Mg-rich zones of Tur investigated in this study (Type-I) are interpreted to have formed around detrital grains on the prograde path, while Fe-rich rims formed on the retrograde path during rehydration. Type-II Tur shows very-high δ^{11}B values, is also related to rehydration, and occurs in paragenesis with chlorite and albite (Marschall et al. 2006). Mineral reactions shown for orientation are taken from Bucher and Frey (1994)

Tourmaline in siliceous marble SY432

Tourmaline in sample SY432 also contains rounded cores with chemical compositions different from the surrounding euhedral rims of the grains. In contrast to sample SY314, the chemical and the B isotopic compositions of individual grains are significantly different from one another with δ^{11}B values differing by more than 14‰ (−10.7 to +3.6‰). Therefore, it can be ruled out that the different tourmaline cores grew in a uniform chemical and B isotopic environment, i.e. in the same rock. The most plausible explanation for the observed variety in tourmaline core compositions is a contribution of detrital tourmaline from a heterogeneous source to the former sediment. Euhedral rims of all grains analysed in sample SY432 are very similar in chemistry and B isotopic composition and show δ^{11}B values of +0.9 ± 1.8‰. These rims are interpreted as prograde or peak metamorphic overgrowths on the detrital cores. Hence, their δ^{11}B value is thought to be characteristic for the peak metamorphic stage of tourmaline in sample SY432. Fe-rich rims were not observed on tourmaline in this sample, and no increase in δ^{11}B values has been found. Hence, the rock was not influenced by retrograde influx of B-bearing fluids.

Boron isotope signatures of terrigenous and marine sediments

The B isotopic composition of continental crust and terrigenous sediments (∼−10‰) is distinctly lighter than the composition of altered oceanic crust (AOC; ∼+5‰) (Leeman and Sisson 2002). Terrigenous clay (illite) found in marine sediments still comprises lighter B (−16 to −3‰) (Ishikawa and Nakamura 1993; Leeman and Sisson 2002) than marine smectite formed during alteration of basalts (−2 to +10‰) (Spivack et al. 1987; Leeman and Sisson 2002). Therefore, it has been suggested before that fluids expelled from subducted sediments or AOC could be discriminated by their B isotopic composition (Bebout and Nakamura 2003). Accordingly, tourmaline formed in metamorphosed terrigenous sediments or AOC during subduction should still record the B isotopic composition of the respective rock type. The δ^{11}B values between −15 and −10‰ for peak metamorphic tourmaline from metasediments from Sambagawa, the Catalina schists and from Lago di Cignana (Nakano and Nakamura 2001; Bebout and Nakamura 2003) are in accordance with the terrigenous character of their protoliths. SY314 and SY432, however, display major-element and modal compositions that are in agreement with protoliths blended from terrigenous and marine contributions. The δ^{11}B values of prograde to peak metamorphic tourmaline in samples SY314 (−1.6‰) and SY432 (+0.9‰) are significantly higher than values from Sambagawa, Catalina and Cignana. Thus, it can be concluded for the Syros samples that the two different sedimentary sources have both influenced the B isotopic composition of the rocks and of the metamorphic tourmaline.

Including tourmaline boron isotopes in provenance studies

The aim of provenance studies is the identification and characterisation of various sources of a sedimentary unit, and its correlation with other sediments. Heavy minerals, such as rutile, zircon and tourmaline, which are highly stable during sedimentation and diagenesis, have been extensively used to approach this aim. Conventional provenance studies compare relative and absolute abundances of the different minerals in order to characterise the sediment, and consider bulk analyses of mineral separates. More advanced provenance studies include structural, morphological, optical and chemical analyses of minerals,

revealing more detailed information on the sources of sediments (Zack et al. 2004; Mange and Otvos 2005; Morton et al. 2005). The high stability of tourmaline during diagenetic and metamorphic processes together with its low intracrystalline diffusivity makes it an ideal monitor during provenance studies not only in sediments and sedimentary rocks, but also in metamorphic rocks (Henry and Guidotti 1985; Henry and Dutrow 2002). In situ analyses of B isotopes in tourmaline from Syros metasediments demonstrate that tourmaline is also a reliable isotopic archive, which can be deciphered in great detail using SIMS, requiring relatively little sample preparation (polished thin sections or grain mounts) and short analyses times ($\sim$10 min per spot). Therefore, the analysis of B isotopes in sedimentary and metasedimentary tourmaline could be a practical tool in provenance studies.

Conclusions

(1) Zones in individual tourmaline grains from H*P* metasedimentary rocks were demonstrated to be of different origins, such as detrital, metamorphic and metasomatic (Fig. 7). The correlation of such zones to their different formation processes is essential for an unambiguous interpretation of tourmaline trace-element and isotope signatures. This condition complied, the different zones can be used to characterise fluids that interacted with the H*P* metasediments at various stages of their *P*–*T* path.

(2) The contrasting δ^{11}B values of detrital cores in the siliceous marble (sample SY432) demonstrate that B isotope inhomogeneities are preserved during low- and medium-grade metamorphism even in small grains ($\sim$20 μm). Therefore, in situ B isotope analysis of tourmaline by SIMS could be employed as a tool for provenance studies not only in sediments, but also in metasediments.

(3) Metamorphic tourmaline from Syros, formed in metamorphic mixed terrigenous-marine sediments, reflects a B isotope signal influenced by these two different sources. δ^{11}B values of prograde to peak metamorphic tourmaline from Syros are significantly higher than values reported from tourmaline in terrigenous sediments from other localities. Therefore, the B isotopic composition of tourmaline from metasedimentary rocks can probably be used to distinguish between terrigenous precursor rocks, altered oceanic crust and mixed lithologies.

Acknowledgments This paper benefited from discussions with Vincent van Hinsberg, Stefan Prowatke and Thomas Zack, and resulted from the Dr. rer. nat. thesis of H.M., which was financially supported by the Deutsche Forschungsgemeinschaft (DFG, grants KA 1023/8-1 and AL 166/15-3). Constructive reviews by Simone Kasemann and Robert Trumbull are acknowledged, as well as editorial handling by Jochen Hoefs.

References

Alt JC, Honnorez J, Laverne C, Emmermann R (1986) Hydrothermal alteration of a 1 km section through the upper oceanic crust, DSDP Hole 504B: mineralogy, chemistry, and evolution off seawater-basalt interactions. J Geophys Res 91:10309–10335

Altherr R, Topuz G, Marschall H, Zack T, Ludwig T (2004) Evolution of a tourmaline-bearing lawsonite eclogite from Elekdag area (Central Pontides, N Turkey): evidence for infiltration of slab-derived B-rich fluids during exhumation. Contrib Mineral Petrol 148:409–425

Bebout GE, Nakamura E (2003) Record in metamorphic tourmaline of subduction-zone devolatilization and boron cycling. Geology 31:407–410

Brady JB, Markley MJ, Schumacher JC, Cheney JT, Bianciardi GA (2004) Aragonite pseudomorphs in high-pressure marbles of Syros, Greece. J Struct Geol 26:3–9

Bröcker M, Enders M (2001) Unusual bulk-rock compositions in eclogite-facies rocks from Syros and Tinos (Cyclades, Greece): implications for U-Pb zircon geochronology. Chem Geol 175:581–603

Bröcker M, Keasling A (2006) Ionprobe U-Pb zircon ages from the high-pressure/low-temperature mélange of Syros, Greece: age diversity and the importance of pre-Eocene subduction. J Met Geol 24:615–631

Bröcker M, Pidgeon RT (2007) Protolith ages of meta-igneous and metatuffaceous rocks from the Cycladic blueschist unit, Greece: results of a reconnaissance U-Pb zircon study. J Geol 115:83–98

Bucher K, Frey M (1994) Petrogenesis of metamorphic rocks, 6th edn. Springer, Heidelberg

Catanzaro FJ, Champion CE, Garner EL, Marinenko G, Sappenfield KM, Shields WR (1970) Boric acid: isotopic and assay standard reference materials. NBS (US) Spec Publ 260:1–70

Chaussidon M, Appel PWU (1997) Boron isotopic composition of tourmalines from the 3.8-Ga-old Isua supracrustals, West Greenland: implications on the Delta^{11}B value of early Archean seawater. Chem Geol 136:171–180

Dixon JE (1968) The metamorphic rocks of Syros, Greece. PhD thesis, St John's College, Cambridge

Dixon JE, Ridley J (1987) Syros. In: Helgeson HC (ed) Chemical transport in metasomatic processes, vol 218 of NATO ASI Series C, Math Phys Sci 489–501, Reidel, Dordrecht

Dutrow BL, Foster CT Jr, Henry DJ (1999) Tourmaline-rich pseudomorphs in sillimanite zone metapelites: demarcation of an infiltration front. Am Mineral 84:794–805

Dyar MD, Taylor ME, Lutz TM, Francis CA, Guidotti CV, Wise M (1998) Inclusive chemical characterization of tourmaline: Mössbauer study of Fe valence and site occupancy. Am Mineral 83:848–864

Dyar MD, Guidotti CV, Core DP, Wearn KM, Wise MA, Francis CA, Johnson K, Brady JB, Robertson JD, Cross LR (1999) Stable isotope and crystal chemistry of tourmaline across pegmatite-country rocks boundaries at Black Mountain and Mount Mica, southwestern Maine, USA. Eur J Mineral 11:281–294

Dyar MD, Wiedenbeck M, Robertson D, Cross LR, Delaney JS, Ferguson K, Francis CA, Grew ES, Guidotti CV, Hervig RL, Hughes JM, Husler J, Leeman W, McGuire AV, Rhede D, Rothe H, Paul RL, Richards I, Yates M (2001) Reference minerals for the microanalysis of light elements. Geostand Newsl 25:441–463

Forster MA, Lister GS (2005) Several distinct tectono-metamorphic slices in the Cycladic eclogite–blueschist belt, Greece. Contrib Mineral Petrol 150:523–545

Frei R, Pettke T (1996) Mono-sample Pb–Pb dating of pyrrhotite and tourmaline: Proterozoic vs. Archean intracratonic gold mineralization in Zimbabwe. Geology 24:823–826

Hecht J (1984) Geological map of Greece 1:50 000, Syros island. Institute of Geology and Mineral Exploration, Athens

Henry DJ, Dutrow BL (1994) Tourmaline in metamorphic rocks: A monitor of boron flux. Geol Soc Am Abstr Prog 26:A449

Henry DJ, Dutrow BL (2002) Metamorphic tourmaline and its petrologic applications. In: Grew ES, Anovitz LM (eds) Boron: mineralogy, petrology and geochemistry, vol 33 of Rev Mineral, 2nd edn., chap 10. Mineralogical Society of America, Washington DC, pp 503–557

Henry DJ, Guidotti CV (1985) Tourmaline as a petrogenetic indicator mineral: an example from the staurolite-grade metapelites of NW Maine. Am Mineral 70:1–15

van Hinsberg VJ, Marschall HR (2007) Boron isotope and light element sector zoning in tourmaline: implications for the formation of B-isotopic signatures. Chem Geol 238:141–148

van Hinsberg VJ, Schumacher JC (2007) Intersector element partitioning in tourmaline: a potentially powerful single crystal thermometer. Contrib Mineral Petrol 153:289–301

Hubert JF (1962) A zircon-tourmaline-rutile maturity index and the independence of the composition of heavy mineral assemblage with the gross composition and texture of sandstones. J Sediment Petrol 32:440–450

Ishikawa T, Nakamura E (1993) Boron isotope systematics of marine sediments. Earth Planet Sci Lett 117:567–580

Jiang S-Y (1998) Stable and radiogenic isotope studies of tourmaline: an overview. J Czech Geol Soc 43:75–90

Kalt A, Schreyer W, Ludwig T, Prowatke S, Bernhardt HJ, Ertl A (2001) Complete solid solution between magnesian schorl and lithian excess-boron olenite in a pegmatite from the Koralpe (eastern Alps, Austria). Eur J Mineral 13:1191–1205

Keay S (1998) The geological evolution of the Cyclades, Greece: constraints from SHRIMP U-Pb geochronology. PhD thesis, Australian National University, Canberra

Keiter M, Piepjohn K, Ballhaus C, Bode M, Lagos M (2004) Structural development of high-pressure metamorphic rocks on Syros island (Cyclades, Greece). J Struct Geol 26:1433–1445

King RW, Kerrich R (1989) Strontium isotope composition of tourmaline from gold lode deposits of the Archean Abitibi Greenstone Belt (Ontario–Quebec, Canada): implications for source reservoirs. Chem Geol 79:225–240

Kretz R (1983) Symbols for rock-forming minerals. Am Mineral 68:277–279

Lagos M, Münker C, Tomaschek F, Ballhaus C, Scherer EE (2003) The age of oceanic crust and of HP/LT-metamorphism on Syros (Cyclades, Greece) based on Lu–Hf geochronology and geochemistry. Geophys Res Abstr 5:12851

Leeman WP, Sisson VB (2002) Geochemistry of boron and its implications for crustal and mantle processes. In: Grew ES, Anovitz LM (eds) Boron: mineralogy, petrology and geochemistry, vol 33, 2nd edn. Mineralogical Society of America, Washington DC, pp 645–708

Leeman WP, Tonarini S (2001) Boron isotopic analysis of proposed borosilicate mineral reference samples. Geostand Newsl 25:399–403

Li R, Li S, Jin F, Wan Y, Zhang S (2004) Provenance of Carboniferous sedimentary rocks in the northern margin of Dabie Mountains, central China and the tectonic significance: constraints from trace elements, mineral chemistry and SHRIMP dating of zircons. Sediment Geol 166:245–264

Lihou JC, Mange-Rajetzky MA (1996) Provenance of the Sardona Flysch, eastern Swiss Alps: example of high-resolution heavy mineral analysis applied to an ultrastable assemblage. Sediment Geol 105:141–157

Maloney J (2007) Lithium and lithium isotopes in tourmaline as indicators of crystallization processes: a study of San Diego County pegmatites, California. Master's thesis, University of Missouri-Columbia, USA

Maluski H, Bonneau M, Kienast JR (1987) Dating the metamorphic events in the Cycladic area: $^{40}Ar/^{39}Ar$ data from metamorphic rocks of the island of Syros (Greece). Bull Soc Geol Fr 8: 833–842

Mange MA, Otvos EG (2005) Gulf coastal plain evolution in west Louisiana: heavy mineral provenance and Pleistocene alluvial chronology. Sed Geol 182:29–57

Marschall HR (2005) Lithium, beryllium, and boron in high-pressure metamorphic rocks from Syros (Greece). Dr. rer. nat. thesis, University of Heidelberg, Germany

Marschall HR, Ludwig T (2006) Re-examination of the boron isotopic composition of tourmaline from the Lavicky granite, Czech Republic, by secondary ion mass spectrometry: back to normal. Critical comment on "Chemical and boron isotopic composition of tourmaline from the Lavicky leucogranite, Czech Republic" by S-Y Jiang et al., Geochemical Journal, 37, 545-556, 2003. Geochem J 40:631–638

Marschall HR, Ludwig T, Altherr R, Kalt A, Tonarini S (2006) Syros metasomatic tourmaline: evidence for very high-$\delta^{11}B$ fluids in subduction zones. J Petrol 47:1915–1942

Meyer C, Wunder B, Meixner A, Romer R, Heinrich W (2007) Experimental study on the B-isotope fractionation between tourmaline and fluid: a re-investigation. Suppl Iss Geochim Cosmochim Acta 71:A659

Morton AC, Whitham AG, Fanning CM (2005) Provenance of Late Cretaceous to Paleocene submarine fan sandstones in the Norwegian Sea: integration of heavy mineral, mineral chemical and zircon age data. Sediment Geol 182:3–28

Nakano T, Nakamura E (2001) Boron isotope geochemistry of metasedimentary rocks and tourmalines in a subduction zone metamorphic suite. Phys Earth Planet Inter 127:233–252

Okrusch M, Bröcker M (1990) Eclogites associated with high-grade blueschists in the Cyclades archipelago, Greece: a review. Eur J Mineral 2:451–478

Palmer MR (1991) Boron isotope systematics of hydrothermal fluids and tourmalines: a synthesis. Chem Geol 94:111–121

Palmer MR, Swihart GH (2002) Boron isotope geochemistry: an overview. In: Grew ES, Anovitz LM (eds) Boron: mineralogy, petrology and geochemistry, vol 33 of Rev Mineral, 2nd edn, chap 13. Mineralogical Society of America, Washington DC, pp 709–744

Reinecke T (1998) Prograde high- to ultrahigh-pressure metamorphism and exhumation of oceanic sediments at Lago di Cignana, Zermatt-Saas Zone, western Alps. Lithos 42:147–189

Ridley J (1984) Evidence for temperature-dependent 'blueschist' to 'eclogite' transformation in high-pressure metamorphism of metabasic rocks. J Petrol 25:852–870

Rosenbaum G, Avigad D, Sánchez-Gómez M (2002) Coaxial flattening at deep levels of orogenic belts: evidence from blueschists and eclogites on Syros and Sifnos (Cyclades, Greece). J Struct Geol 24:1451–1462

Seck HA, Kötz J, Okrusch M, Seidel E, Stosch HG (1996) Geochemistry of a meta-ophiolite suite: an association of metagabbros, eclogites and glaucophanites on the island of Syros, Greece. Eur J Mineral 8:607–623

Slack JF (2002) Tourmaline associations with hydrothermal ore deposits. In: Grew ES, Anovitz LM (eds) Boron: mineralogy, petrology and geochemistry, vol 33 of Rev Mineral, 2nd edn.,

chap 11. Mineralogical Society of America, Washington DC, pp 559–644

Slack JF, Palmer MR, Stevens BP, Barnes RG (1993) Origin and significance of tourmaline-rich rocks in the Broken Hill district, Australia. Econ Geol 88:505–541

Smith M, Yardley BWD (1994) The boron isotopic composition of tourmaline as a guide to fluid processes and boron source in the South-west England orefield: an ion microprobe study. Mineral Mag 58A:856–857

Spivack AJ, Palmer MR, Edmond JM (1987) The sedimentary cycle of the boron isotopes. Geochim Cosmochim Acta 51:1939–1949

Thiel GA (1941) The relative resistance to abrasion of mineral grains of sand size. J Sediment Petrol 10:103–124

Tomaschek F, Kennedy AK, Villa IM, Lagos M, Ballhaus C (2003) Zircons from Syros, Cyclades, Greece—recrystallization and mobilization of zircon during high-pressure metamorphism. J Petrol 44:1977–2002

Trotet F, Vidal O, Jolivet L (2001) Exhumation of Syros and Sifnos metamorphic rocks (Cyclades, Greece). New constraints on the *P–T* paths. Eur J Mineral 13:901–920

Werding G, Schreyer W (2002) Experimental studies on borosilicates and selected borates. In: Grew ES, Anovitz LM (eds) Boron: mineralogy, petrology and geochemistry, vol 33 of Rev Mineral, 2nd edn. Mineralogical Society of America, pp 117–163

Zack T, von Eynatten H, Kronz A (2004) Rutile geochemistry and its potential use in quantitative provenance studies. Sediment Geol 171:37–58